



Initiating Electron Transfer in Doubly Curved Nanographene Upon Supramolecular Complexation of C₆₀

Simon Zank⁺, Jesús M. Fernández-García⁺, Anton J. Stasyuk, Alexander A. Voityuk, Marcel Krug, Miquel Solà,* Dirk M. Guldi,* and Nazario Martín*

Dedicated to Professor Tomás Torres on the occasion of his 70th birthday

Abstract: The formation of supramolecular complexes between C₆₀ and a molecular nanographene endowed with both positive and negative curvatures is described. The presence of a corannulene moiety and the saddle shape of the molecular nanographene allows the formation of complexes with 1:1, 1:2, and 2:1 stoichiometries. The association constants for the three possible supramolecular complexes were determined by ¹H NMR titration. Furthermore, the stability of the three complexes was calculated by theoretical methods that also predict the photoinduced electron transfer from the curved nanographene to the electron acceptor C₆₀. Time-resolved transient absorption measurements on the ns-time scale showed that the addition of C₆₀ to NG-I solutions and photo-exciting them at 460 nm leads to the solvent-dependent formation of new species, in particular the formation of the one-electron reduced form of C₆₀ in benzonitrile was observed.

Introduction

Graphene quantum dots are electron confined flakes of graphene with dimensions usually in the 3–20 nm range. They are considered as a singular family of zero dimensional (0D) carbon-based materials, since, in contrast to pristine graphene, these nanomaterials are luminescent with a non-zero band gap stemming from quantum confinement and edge effects.^[1] By virtue of such unique electronic features, they render outstanding materials for optoelectronic devices,^[2] energy storage systems,^[3] perovskite solar cells,^[4] and biomedical applications.^[5]

In recent years, bottom-up approaches have enabled solution-phase syntheses of these materials in a step-by-step fashion. This has resulted in an accurate control over size,

morphology and, therefore, on-demand fine-tuning of the properties.^[6] Molecular nanographenes with a wide range of shapes, namely bilayers,^[7] belts,^[8] ribbons,^[9] propellers,^[10] helical,^[11] planar^[12] and curved,^[13] have been prepared by using controlled bottom-up approaches (Figure 1).

Synthetic implementation of defects such as non-hexagonal rings into the 2D honey-comb lattice endows Gaussian

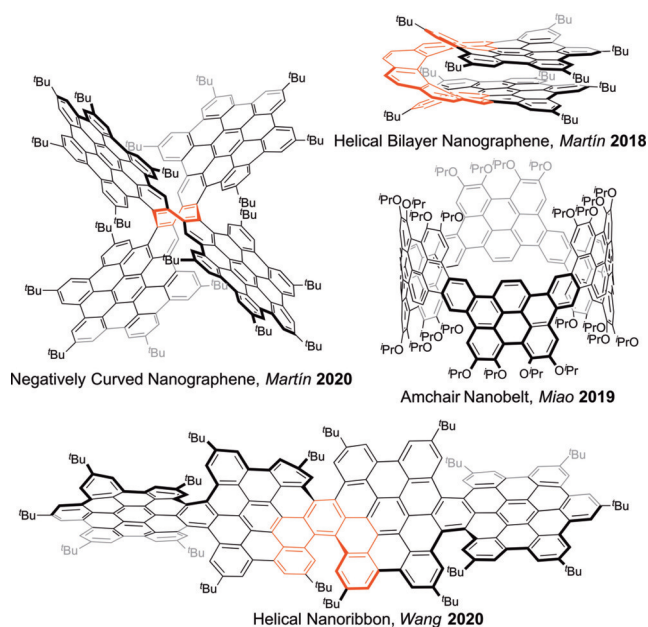


Figure 1. Recent examples of nanographenes with different topologies synthesized by bottom-up approach.

[*] S. Zank,^[†] M. Krug, Prof. Dr. D. M. Guldi
 Department of Chemistry and Pharmacy
 Friedrich-Alexander-Universität
 Egerlandstrasse 3, 91058 Erlangen (Germany)
 E-mail: dirk.guldi@fau.de

Dr. J. M. Fernández-García,^[†] Prof. Dr. N. Martín
 Departamento de Química Orgánica I, Facultad de Ciencias
 Químicas, Universidad Complutense de Madrid
 Avd. de la Complutense, S/N, 28040 Madrid (Spain)
 E-mail: nazmar@ucm.es

Dr. A. J. Stasyuk, Prof. Dr. A. A. Voityuk, Prof. Dr. M. Solà
 Institut de Química Computacional and Departament de Química,
 Universitat de Girona
 C/ Maria Aurèlia Capmany 69, 17003 Girona (Spain)
 E-mail: miquel.sola@udg.edu

Prof. Dr. A. A. Voityuk
 Institució Catalana de Recerca i Estudis Avançats (ICREA)
 08010 Barcelona (Spain)
 Prof. Dr. N. Martín
 IMDEA-Nanociencia
 C/ Faraday, 9, Campus de Cantoblanco, 28049 Madrid (Spain)

[†] These authors contributed equally to this work.

Supporting information and the ORCID identification number(s) for the author(s) of this article can be found under:
 https://doi.org/10.1002/anie.202112834.

© 2021 The Authors. Angewandte Chemie International Edition published by Wiley-VCH GmbH. This is an open access article under the terms of the Creative Commons Attribution License, which permits use, distribution and reproduction in any medium, provided the original work is properly cited.

curvature to molecular nanographenes. Introducing five- or four-membered rings leads to positive Gaussian curvature affording bowl shape morphologies. In contrast, inserting rings larger than hexagons involves the formation of negative Gaussian curvature and implies saddle shape structures. No doubt, the co-existence of both curvature motifs in molecular nanographenes is extraordinary. Thus, the syntheses and properties of several nanographenes with a combined bowl and saddle shape have been reported in the literature.^[14]

Recently, our research group has described the synthesis of corannulene-based nanographenes featuring both positive and helical or negative curvatures.^[15] This procedure is based on the π -extension of positively curved bromocorannulene by sequential Sonogashira, Diels–Alder, and Scholl reactions. Oxidant-dependent and selective Scholl closure of a seven-membered ring leads to a positively and simultaneously negatively curved molecular nanographene **NG-1** or to a positive-curved helical molecular nanographene **NG-2** when the ring closure does not take place (Figure 2).

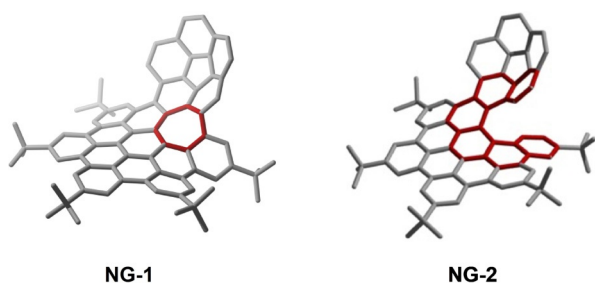


Figure 2. π -extended corannulene-based curved nanographenes **NG-1** and **NG-2**.

Curvature of nanographene **NG-1** renders it a unique host for the complexation of fullerenes, driven by concave-convex interactions. As a matter of fact, complexation by any negatively curved nanographenes remains poorly explored. In addition, the electron-accepting nature of C_{60} gives rise to discernible electronic communication with, for example, suitable electron donors, especially under light irradiation.^[16]

In the current contribution, we report on results regarding static and dynamic interactions between **NG-1** and C_{60} . The combination of these two compounds creates a system which is solely based on carbon and hydrogen. Furthermore, theoretical calculations underpin the stability of the different complexes and predict that photoinduced electron transfer occurs in the picosecond timescale. Nanosecond time-resolved assays pointed out the tunability of the dynamic processes. In polar benzonitrile, electron transfer from the curved nanographene to C_{60} leading to the formation of the respective radical-ion pair is observed. In less polar chlorobenzene, the radical ion pair cannot be stabilized and triplet excited state energy transfer from **NG-1** to C_{60} remains.

Results and Discussion

As aforementioned, curved **NG-1** and **NG-2** have been synthesized by Sonogashira–Diels–Alder–Scholl sequential

reactions.^[16] The aim of this work is focused on the supramolecular complexation of **NG-1** with C_{60} by taking advantage of their respective concave and convex geometries.^[17]

Experimental corroboration for the complexation of, for example, curved **NG-1** and C_{60} was performed by $^1\text{H-NMR}$ titration. In an NMR sample tube, a 5×10^{-4} M $[\text{D}_8]$ toluene solution of **NG-1** was prepared. Sequential additions of a solution of C_{60} (2×10^{-3} M) and **NG-1** (5×10^{-4} M) resulted in $^1\text{H-NMR}$ spectra, which are shown in Figure 3a. Several signals shift down-field and prompt to the successful formation of **NG-1**· C_{60} . In this way, signals at $\delta = 9.36$ (H_a) and $\delta = 7.91$ (H_d) underwent shifts to lower fields by $\Delta\delta H_a = -0.02$ ppm and $\Delta\delta H_d = -0.05$ ppm, respectively. Signals at $\delta = 9.24$ (H_b) and $\delta = 8.76$ (H_c) experienced shifts to higher fields $\Delta\delta H_b = 0.04$ ppm and $\Delta\delta H_c = 0.05$ ppm. 2D-NMR experiments were used to assign these signals (Figure 3b). H_a , H_c , and H_d match those protons, which are located at the interface between the corannulene and the rest of the π -system. In other words, in close proximity to the seven-membered ring, where the curvature is most significant, and where concave-convex interactions between **NG-1** and C_{60} are strongest.

The association constants have been calculated taking three different complex stoichiometries, namely 1:1 (**NG-1**· C_{60}), 1:2 (**NG-1**·(C_{60})₂), and 2:1 ((**NG-1**)₂· C_{60}), into account. Considering a 1:1 stoichiometry in **NG-1**· C_{60} , complexes are formed between the π -system containing the concave surface of corannulene and C_{60} by means of concave-convex interactions. Here, the proton-shifts for H_a , H_b , H_c , and H_d fit with the model with a low value of Sum of Squared Residuals $\text{SSR}_{1:1} = 1.0024 \times 10^{-4}$. From this, we conclude a rather tight fit of the model with the data. In this model, the calculated association constant is $K_a = 1.17 \times 10^3 \text{ M}^{-1}$ and the mole fraction of **NG-1**· C_{60} is 0.5 when 2.2 equivalents of C_{60} were added (Figure S2).

For **NG-1**·(C_{60})₂, additionally to the aforementioned interactions in **NG-1**· C_{60} , a second set of concave-convex interactions occur at, however, the opposite face of **NG-1**. It is based on the negative curvature that confers the saddle-shape of **NG-1**. CH- π interactions between $t\text{Bu}$ groups of **NG-1** and C_{60} are likely to play an important role. The data fit brings $\text{SSR}_{1:2} = 5.42 \times 10^{-5}$, which is somewhat better than the 1:1 stoichiometry fittings. The calculated association constants are $K_{a1} = 1.69 \times 10^3 \text{ M}^{-1}$ and $K_{a2} = 1.16 \times 10^3 \text{ M}^{-1}$. Lastly, a 2:1 stoichiometry model was studied. (**NG-1**)₂· C_{60} implies a complexation between the π -extended concave face of corannulene of two molecules of **NG-1** and one C_{60} . Overall, the fullerene remains inside the nanographene cage ($\text{SSR}_{2:1}$ is 5.14×10^{-5}). From the calculated association constants of $K_{a1} = 1.71 \times 10^3 \text{ M}^{-1}$ and $K_{a2} = 3.17 \times 10^3 \text{ M}^{-1}$ we derive the coexistence of three plausible species **NG-1**· C_{60} , **NG-1**·(C_{60})₂, and (**NG-1**)₂· C_{60} in almost the same concentration when about 1.5 equivalents of C_{60} were added (Figure S4).

For **NG-1**· C_{60} , two conformers are possible. The first isomer is formed by non-covalent interactions between C_{60} and the concave surface of corannulene, whereas in the second isomer C_{60} interacts with the saddle-shaped surface on the opposite side of **NG-1**. The latter is $7.9 \text{ kcal mol}^{-1}$ less

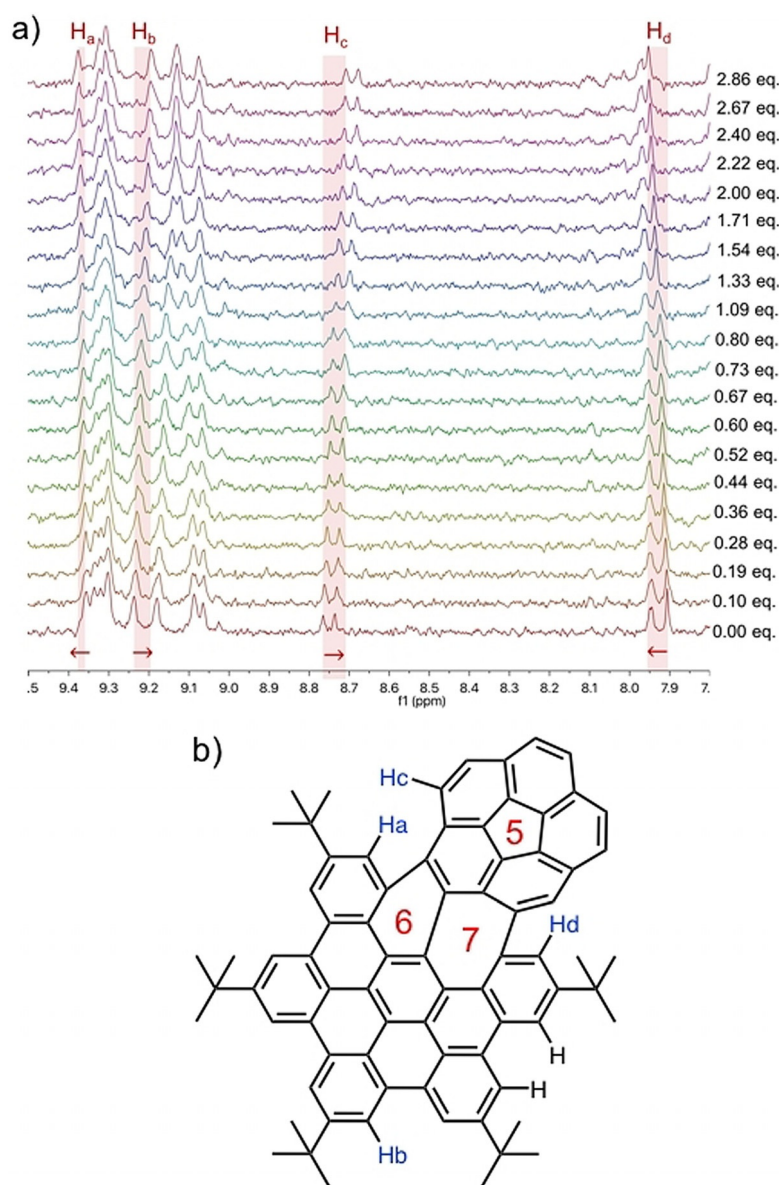


Figure 3. a) ^1H NMR spectra of **NG-1** with sequential additions of C_{60} . b) Signal assignment of **NG-1** by 2D NMR experiments.

stable than the former according to our calculations (Figure S5, SI). In **NG-1**·(C_{60})₂ complex, each side of **NG-1** interacts with one C_{60} , thus only one isomer is possible, while for (**NG-1**)₂· C_{60} multiple isomers with different mutual orientations of the fragments we found. Figure S5, SI, depicts several isomers found for these complexes. The relative stability of the conformers of **NG-1**· C_{60} , **NG-1**·(C_{60})₂, and (**NG-1**)₂· C_{60} complexes in the ground state (GS) was assessed by DFT calculations at the BLYP-D3(BJ)/def2-SVP level of theory^[18] (see SI for details). The structures of the most stable conformers are shown in Figure 4.

To estimate the stability of each complex, the interaction energies (ΔE_{int}) between **NG-1** and C_{60} were computed. For the most stable conformers of **NG-1**· C_{60} , **NG-1**·(C_{60})₂, and (**NG-1**)₂· C_{60} , ΔE_{int} is found to be -39.83 , -66.98 , and -84.94 kcal mol⁻¹, respectively. We infer that these interac-

tion energies are somewhat overestimated. For **NG-1**· C_{60} , accounting for the basis set superposition error (BSSE) reduces the interaction energy by ca. 2 kcal mol⁻¹, whereas the use of hybrid and range corrected functionals results in lower stabilization energies, which vary in the range from 5 to 9 kcal mol⁻¹, (Table S2, SI). Similar to previously reported carbon-rich complexes,^[19] the interaction energy in (**NG-1**)₂· C_{60} is superadditive. In particular, the total stabilization energy is 5 kcal mol⁻¹ larger than the sum of interaction energies in two **NG-1**· C_{60} (Figure S6, SI).

Taking into account the electron acceptor properties of C_{60} , we looked at the charge separation between **NG-1** and C_{60} in the ground state. The population analysis provides no evidence for significant charge transfer between the fragments (Table S3, SI). In addition, we performed an energy decomposition analysis (EDA), which enables to divide the interaction energy into four components: electrostatic (ΔE_{elstat}), Pauli repulsion (ΔE_{Pauli}), orbital (ΔE_{orb}), and dispersion correction (ΔE_{disp}) (Table S4, SI). Binding forces in these complexes were found to be similar. The largest contribution to the attraction between the two constituents is the dispersion term (around 60%), which is followed by the electrostatic term (26–29%) and the orbital interaction term (13–15%). The topology of the non-covalent interactions was described using the NCI calculations^[20] (Figures S7 and S8, SI).

The simulation of the lowest 80 excited states was carried out by the TDA-DFT method with the CAM-B3LYP-D3(BJ)/def2-SVP//BLYP-D3(BJ)/def2-SVP Scheme.^[18c,21] To characterize the excited states, the complexes were divided into **NG-1** and C_{60} fragments (two in the case of **NG-1**· C_{60} or three in the cases of **NG-1**·(C_{60})₂ and (**NG-1**)₂· C_{60}). Within this Scheme, three types of excited states can be identified: (1) locally excited (LE) states, in

which the excitation is mainly localized only on a single fragment and the degree of charge separation is less than 0.1

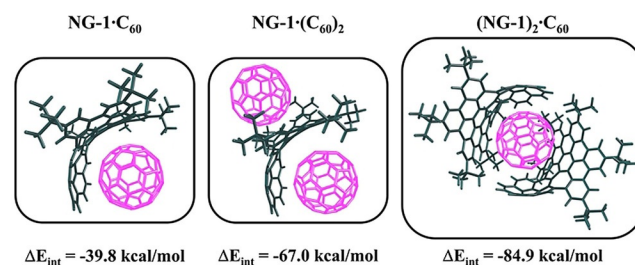


Figure 4. Optimized structures and interaction energies of the most stable conformers obtained at the BLYP-D3(BJ)/def2-TZVP//BLYP-D3(BJ)/def2-SVP level of theory.

e (CS value $< 0.1 e$); (2) charge separated (CS) states with a significant amount of electron density transferred between the fragments (CS value $> 0.8 e$) and (3) mixed states with a significant contribution of both LE and CS ($0.1 e < \text{CS value} < 0.8 e$).

In the gas phase, the excitation energies range from 2.46 to 4.25 eV (Table S5, SI). In all complexes, the LE state on C_{60} (LE_1) has the lowest energy. The LE states with an exciton on **NG-1** (LE_2) are 0.58–0.65 eV higher in energy. Among the 80 lowest excited states, we found only CS states that correspond to the electron transfer from **NG-1** to C_{60} . The energy of the lowest CS state varies slightly from 2.65 to 2.72 eV depending on the stoichiometry of the complex. The direct population of the CS states due to light absorption is unlikely due to their low oscillator strength (f) of < 0.001 . However, the CS states can be generated by the decay of LE states. The highly absorptive states, with an oscillator strength ranging from 0.32 to 0.74 are found in the complexes at 3.83–3.89 eV (Table S5, SI). The Kohn–Sham molecular orbitals representing the LE and CS states are shown in Figures S9–S11, SI.

A COSMO-like model was applied to estimate the influence of a polar environment on the electronic excitations.^[22] Benzonitrile (BZN) was taken as the solvent. The ground state (GS) solvation energies of **NG-1**· C_{60} , **NG-1**·(C_{60})₂, and (**NG-1**)₂· C_{60} are found to be -0.35 , -0.37 , and -0.67 eV, respectively.

As expected, the dipole moment and solvation energy of the LE_1 and LE_2 states are similar to those in the ground state (Table S6, SI). In contrast, the molecular dipole moment increases considerably as a result of the CS excitations. For **NG-1**· C_{60} , **NG-1**·(C_{60})₂, and (**NG-1**)₂· C_{60} , the $\Delta\mu^{CS}$ is 22.5, 22.4, and 16.1 D, respectively. This in turn leads to a better stabilization of CS states by the polar environment as compared to the LE states (Figure 5). The calculations revealed that the CS state energy in the **NG-1**· C_{60} , **NG-1**·(C_{60})₂, and (**NG-1**)₂· C_{60} complexes decreases by 0.65, 0.63, and 0.89 eV, correspondingly. As seen in Figure 5, the solvent stabilization of the excited states makes the charge separation from LE_1 energetically favorable. The LE state energies differ by less than 0.1 eV when compared to those of isolated C_{60} and **NG-1** units (Table S7, SI).

The rate of electron transfer (k_{ET}) was calculated using the Marcus equation.^[23] Within this approach, the rate is controlled by three parameters: electronic coupling V_{ij} of initial and final states, reorganization energy λ , and reaction Gibbs energy ΔG^0 . Using the computed data listed in Table 1, we estimated the rates for the charge separation.

The charge separation is characterized by a negative ΔG^0 , except for (**NG-1**)₂· C_{60} , where ΔG^0 is almost zero, and it occurs in the normal Marcus regime ($|\Delta G^0| < \lambda$) on the picosecond time scale. Note that the charge transfer reaction in **NG-1**· C_{60} and **NG-1**·(C_{60})₂ is significantly faster than in (**NG-1**)₂· C_{60} .

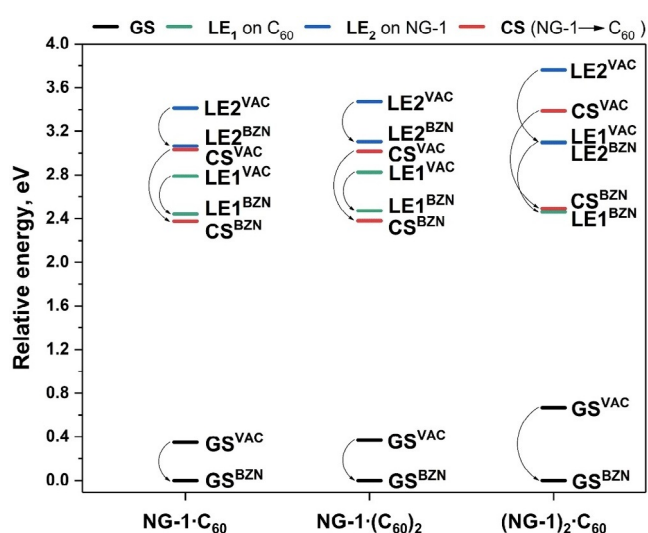


Figure 5. Relative energies of LE and CS states of **NG-1**· C_{60} , **NG-1**·(C_{60})₂, and (**NG-1**)₂· C_{60} complexes computed in vacuum (VAC) and benzonitrile (BZN). The CS states correspond to electron transfer from **NG-1** to C_{60} fragment.

Table 1: Gibbs energy ΔG^0 , electronic coupling $|V_{ij}|$, reorganization energy λ , ET rate k_{ET} , and characteristic time τ for charge separation in the **NG-1**· C_{60} , **NG-1**·(C_{60})₂, and (**NG-1**)₂· C_{60} complexes in benzonitrile.

Complex	Transition	$\Delta G^{0[a]}$ [eV]	$ V_{ij} $ [eV]	Reorg. Energy [eV]	k_{ET} [s^{-1}]	τ [ns]
NG-1 · C_{60}	LE→CS	-0.063	6.01×10^{-3}	0.545	1.30×10^{10}	0.08
NG-1 ·(C_{60}) ₂	LE→CS	-0.091	4.35×10^{-3}	0.440	1.98×10^{10}	0.05
(NG-1) ₂ · C_{60}	LE→CS	0.035	3.40×10^{-3}	0.570	2.10×10^9	0.48

[a] Gibbs energy difference between LE and CS states in benzonitrile.

To shed light onto the photo-physical consequences that stem from the interaction between **NG-1** and C_{60} we turned to steady-state and time-resolved investigations. The starting point were titrations, in which variable amounts of C_{60} up to 4.0×10^{-5} M were added to a constant concentration of **NG-1** (2.0×10^{-6} M) and the absorption differences were subsequently recorded. No particular changes were, however, noted. As a matter of fact, the absorption spectra of **NG-1** in the presence of C_{60} are best described as the simple superimposition of the individual constituents. An independent confirmation came from subtracting any contributions from C_{60} along every step of the titrations. Here, it is simply the unaltered **NG-1** absorptions that are discernible. Quite similar is the outcome of the titrations when following the fluorescence rather than the absorption. In fact, the **NG-1** fluorescence is subject to a minimal decrease, without showing any new fluorescent characteristics. Contributions from inner filter effects rendered it impossible to quantify the static interactions between **NG-1** and C_{60} . Considering the binding constants as they were determined in the NMR experiments (see above) complex formation under the conditions used in our spectroscopic experiments is disfavored.^[24]

Information regarding the dynamic interactions, that is, energy versus electron transfer between **NG-1** and C_{60} , came from time-resolved transient absorption measurements on the

ns-time scale (ns-TAS). Initially, **NG-1** was probed in 460 nm photo-excitation experiments in the absence of any C_{60} (Figure S12, SI). The presence of two dominant species was derived from the ns-TAS 3D heat maps. It is, on the one hand, the singlet excited state of **NG-1** with a maximum at 665 nm. On the other hand, maxima at 550 and 690 nm as well as a minimum at 615 nm are ascribed to the triplet excited state of **NG-1**.

All characteristics concluded from differential absorption spectra are in excellent agreement with the species associated spectra (SAS) obtained from Global Target Analysis. Our two-species model is based on the lowest singlet and triplet excited states. Importantly, any branching coefficients were derived from FQY, while assuming that contributions from internal conversion are minor. All lifetimes are summarized in Table 2.

Adding C_{60} to **NG-1** solutions to realize different **NG-1**-to- C_{60} ratios of 1:5, 1:10 as well as 1:25 and photo-exciting them at 460 nm led to some changes in the ns-TAS 3D heat maps (Figure 6). Both the singlet and triplet excited states of

Table 2: Summary of the transient lifetimes determined by global target analysis for different molar ratios of **NG-1** and C_{60} .^[a]

NG-1- C_{60}	1:0	1:5	1:10	1:15	1:25
Chlorobenzene					
S_1 (NG-1)	4.44 ns	4.44 ns	4.44 ns	–	4.44 ns
T_1 (NG-1)	22.3 μ s	3.90 μ s	2.07 μ s	–	0.87 μ s
T_1 (C_{60})	–	26.8 μ s	16.0 μ s	–	31.4 μ s
Benzonitrile					
S_1 (NG-1)	5.59 ns	5.59 ns	5.59 ns	5.59 ns	5.59 ns
T_1 (NG-1)	>100 μ s	6.07 μ s	4.26 μ s	3.49 μ s	2.69 μ s
$NG-1^{+} \cdot C_{60}^{-}$	–	>100 μ s	>100 μ s	43.5 μ s	22.9 μ s

[a] In chlorobenzene and benzonitrile after laser excitation at 460 nm. The lifetime of the **NG-1** singlet excited state was fixed during the global target analysis, since it only showed small deviations.

NG-1 dominate the 3D heat maps, albeit with somewhat shorter lifetimes for the triplet excited state. As a major change, another species evolved on the long timescales, that is, > 1 μ s. It is linked to the faster decay of the **NG-1** triplet excited state. Intriguingly, an analysis of the 3D heat maps reveals that the nature of this newly formed species is solvent dependent. In chlorobenzene, for example, the spectroscopic fingerprints of the C_{60} triplet excited state are seen to evolve at 750 nm.^[25] In benzonitrile, it is the one-electron reduced form of C_{60} that is identified by its 1080 nm fingerprint (Figure 7).^[26] Global target analyses allowed deconvoluting the spectra for each component. Important is the fact that we took the ratio of the extinction coefficients of **NG-1** and C_{60} at the excitation wavelength to account for the population of the C_{60} triplet excited state via ISC into our model. Such a mechanistic refinement helped in terms of the SAS quality of the **NG-1** singlet and triplet excited states as the first and second species, respectively.^[27]

The SAS of the third species bears in chlorobenzene the features of the C_{60} triplet excited state at 750 nm, while those of the C_{60} radical anion at 1080 nm were noted in benzonitrile.

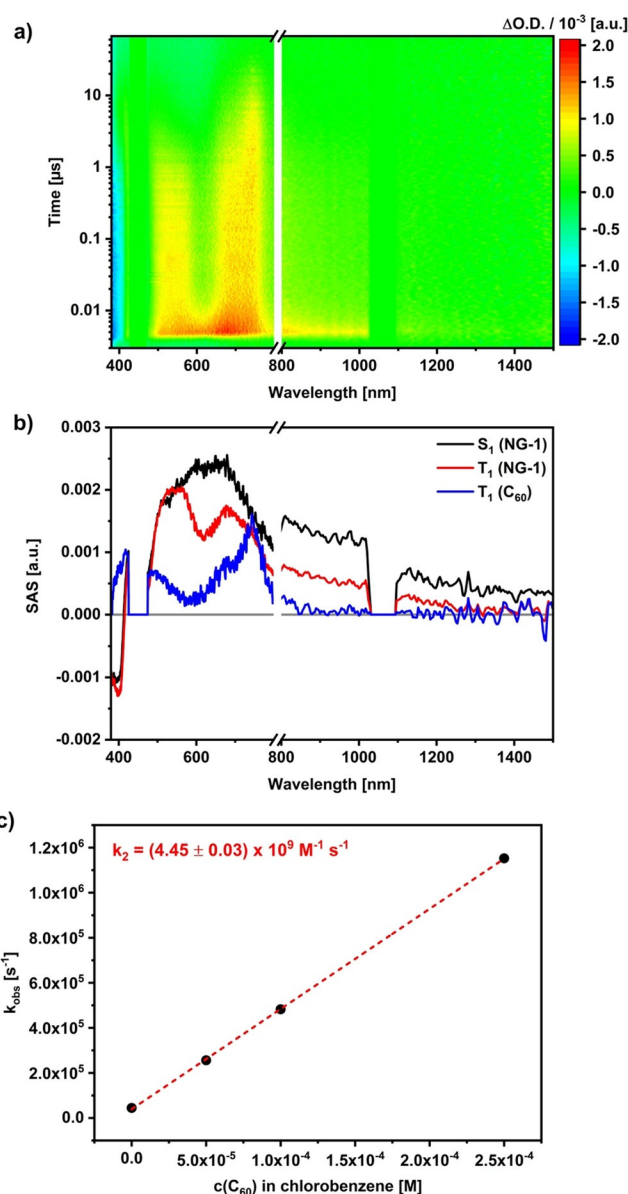


Figure 6. a) Differential transient absorption spectra of **NG-1** (1.0×10^{-5} M) and C_{60} (1.0×10^{-4} M) in a 1:10 molar ratio at time delays between 0 and 70 μ s after laser excitation at 460 nm in argon purged chlorobenzene. b) SAS obtained from global target analysis. c) Determination of the bimolecular rate constant k_2 of the triplet excited state lifetime of **NG-1** with increasing amount of C_{60} .

Using the pseudo first-order rate constants and treating them as a function of C_{60} concentrations afforded second-order rate constants for the energy transfer in chlorobenzene and the electron transfer in benzonitrile of 4.45×10^9 and 1.36×10^9 $M^{-1} s^{-1}$, respectively. Both of them are nearly diffusion-controlled.^[28]

Conclusion

The complexation between a corannulene-based molecular nanographene **NG-1** with both, negative and positive

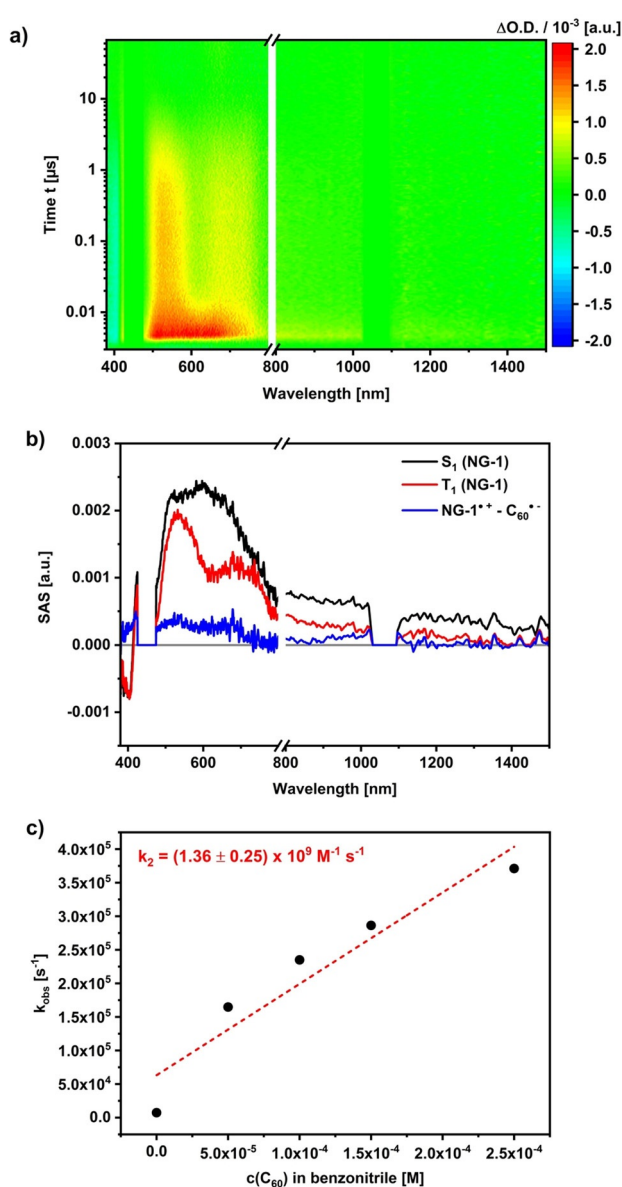


Figure 7. a) Differential transient absorption spectra of **NG-1** (1.0×10^{-5} M) and C_{60} (1.0×10^{-4} M) in a 1:10 molar ratio at time delays between 0 and 70 μ s after laser excitation at 460 nm in argon purged benzonitrile. b) SAS obtained from global target analysis. c) Determination of the bimolecular rate constant k_2 of the triplet excited state lifetime of **NG-1** with increasing amount of C_{60} .

curvature and C_{60} was achieved. The ^1H NMR titration performed by the addition of a solution of C_{60} to a solution of **NG-1** showed the major shift of the protons close to the union between corannulene and the π -extended system, where the curvature is the strongest. Concave-convex interactions between the concave surface of the corannulene moiety of the molecular nanographene and C_{60} can result in the formation of the complex **NG-1**· C_{60} with 1:1 stoichiometry and an association constant $K_a = 1.17 \times 10^3 \text{ M}^{-1}$. Furthermore, the saddle shape gathered by the negative curvature allows the formation of concave-convex interactions with another molecule of C_{60} conducting to the formation of the complex **NG-1**·(C_{60})₂ with 1:2 stoichiometry and association constants

$K_{a1} = 1.69 \times 10^3 \text{ M}^{-1}$ and $K_{a2} = 1.16 \times 10^3 \text{ M}^{-1}$. However, the best fit for the data extracted from the ^1H NMR titration is for the complex (**NG-1**)₂· C_{60} with 2:1 stoichiometry where a C_{60} molecule remains encapsulated between the concave surface of the corannulene of two molecules of **NG-1**. The measured association constants are $K_{a1} = 1.71 \times 10^3 \text{ M}^{-1}$ and $K_{a2} = 3.17 \times 10^3 \text{ M}^{-1}$.

Theoretical calculations of the stability of these complexes were performed computing the interaction energies (ΔE_{int}) between **NG-1** and C_{60} . For the most stable conformers of **NG-1**· C_{60} , **NG-1**·(C_{60})₂, and (**NG-1**)₂· C_{60} , ΔE_{int} is found to be -39.83 , -66.98 , and $-84.94 \text{ kcal mol}^{-1}$, respectively. Furthermore, population analysis lacked any evidence for a significant charge transfer between the fragments in the ground state. However, in the calculations of the excited states for the complexes with the three stoichiometries, we found: 1) locally excited (LE) states, in which the excitation is mainly localized on one fragment 2) Charge separated (CS) states with a significant amount of electron density transferred between the fragments and, 3) mixed states with a significant contribution of both LE and CS. The charge transfer reaction for **NG-1**· C_{60} and **NG-1**·(C_{60})₂ is significantly faster than that for (**NG-1**)₂· C_{60} .

Titration absorption and fluorescence studies do not show the formation of any complex, because the small association energies for the complexation reactions determined by NMR do not allow the complexation under the high dilution conditions of these spectroscopic methods. Time-resolved transient absorption measurements on the ns-time scale of solutions of **NG-1** in the presence of C_{60} indicate solvent dependent, bimolecular processes. In chlorobenzene, it is triplet excited state energy transfer to yield the C_{60} triplet excited state. In polar benzonitrile, the detection of one-electron reduced C_{60} confirms electron transfer.

This study validates the use of curved nanographenes as interesting and singular hosts for further concave-convex supramolecular complexations and paves the way to the use of other nanographenes where shapes can play an essential role. Furthermore, molecular nanographenes exhibit appealing chemical, chiroptical and photophysical properties, which can be skillfully used in the formation of unprecedented non-covalent complexes in the search for amazing controlled properties.

Acknowledgements

The authors J.F.-G. and N.M. acknowledge support from the Spanish Ministry of Science, Innovation and Universities MCIU (Projects CTQ2017-84327-P and CTQ2017-83531-R). A.J.S., A.A.V., and M.S. are grateful for financial support from the Spanish MCIU (Network RED2018-102815-T, projects CTQ2017-85341-P and PID2020-113711GB-I00, and Juan de la Cierva contract IJC2019-039846-I to A.J.S.) and the Catalan DIUE (2017SGR39). We kindly thank Prof. Jay J. Siegel for generously supplying the starting corannulene. We also thank Prof. Pall Thordarson for his valuable comments on the supramolecular fitting software. Open Access funding enabled and organized by Projekt DEAL.

Conflict of Interest

The authors declare no conflict of interest.

Keywords: curved nanographenes · DFT · electron transfer · fullerene · supramolecular complexation

- [1] a) S. Fujii, T. Enoki, *Acc. Chem. Res.* **2013**, *46*, 2202–2210; b) Y. Gu, X. Wu, T. Y. Gopalakrishna, H. Phan, J. Wu, *Angew. Chem. Int. Ed.* **2018**, *57*, 6541–6545; *Angew. Chem.* **2018**, *130*, 6651–6655.
- [2] a) F. Bonaccorso, Z. Sun, T. Hasan, A. Ferrari, *Nat. Photonics* **2010**, *4*, 611–622; b) C. Wang, H. Dong, W. Hu, Y. Liu, D. Zhu, *Chem. Rev.* **2012**, *112*, 2208–2267; c) R. M. Metzger, *Chem. Rev.* **2015**, *115*, 5056–5115.
- [3] a) D. Odkhuu, D. H. Jung, H. Lee, S. S. Han, S.-H. Choi, R. S. Ruoff, N. Park, *Carbon* **2014**, *66*, 39–47; b) H. J. Yen, H. Tsai, M. Zhou, E. F. Holby, S. Choudhury, A. Chen, L. Adamska, S. Tretiak, T. Sanchez, S. Iyer, H. Zhang, L. Zhu, H. Lin, L. Dai, G. Wu, H.-L. Wang, *Adv. Mater.* **2016**, *28*, 10250–10256; c) A. V. Zabula, S. N. Spisak, A. S. Filatov, A. Y. Rogachev, M. A. Petrukhina, *Acc. Chem. Res.* **2018**, *51*, 1541–1549; d) Z. Lu, D. Gao, D. Yi, Y. Yang, X. Wang, J. Yao, *ACS Cent. Sci.* **2020**, *6*, 1451–1459.
- [4] a) J. Cao, Y. M. Liu, X. Jing, J. Yin, J. Li, B. Xu, Y. Z. Tan, N. Zheng, *J. Am. Chem. Soc.* **2015**, *137*, 10914–10917; b) N. Martín, *Adv. Energy Mater.* **2017**, *7*, 1601102; c) J. Urieta-Mora, I. García-Benito, A. Molina-Ontoria, N. Martín, *Chem. Soc. Rev.* **2018**, *47*, 8541–8571.
- [5] a) *Carbon Nanostructures for Biomedical Applications* (Eds.: T. Da Ros, N. Martín, J.-F. Nierengarten), RSC, Cambridge, **2021**; b) Y. Liu, X. Dong, P. Chen, *Chem. Soc. Rev.* **2012**, *41*, 2283–2307; c) L. Rodríguez-Pérez, J. Ramos-Soriano, A. Pérez-Sánchez, B. M. Illescas, A. Muñoz, J. Luczkowiak, F. Lasala, J. Rojo, R. Delgado, N. Martín, *J. Am. Chem. Soc.* **2018**, *140*, 9891–9898; d) I. M. Santos, L. Rodríguez-Pérez, G. Gonçalves, S. N. Pinto, M. Melle-Franco, P. A. A. P. Marques, M. A. F. Faustino, M. A. Herranz, N. Martín, M. G. P. M. S. Neves, J. M. G. Martinho, E. M. S. Mações, *Carbon* **2020**, *166*, 164–174.
- [6] a) X.-Y. Wang, A. Narita, K. Müllen, *Nat. Rev. Chem.* **2018**, *2*, 0100; b) J. M. Fernández-García, P. J. Evans, S. Filippone, M. A. Herranz, N. Martín, *Acc. Chem. Res.* **2019**, *52*, 1565–1574.
- [7] a) Y. Cao, V. Fatemi, S. Fang, K. Watanabe, T. Taniguchi, E. Kaxiras, P. Jarillo-Herrero, *Nature* **2018**, *556*, 43–50; b) P. J. Evans, J. Ouyang, L. Favereau, J. Crassous, I. Fernández, J. Perles Hernández, N. Martín, *Angew. Chem. Int. Ed.* **2018**, *57*, 6774–6779; *Angew. Chem.* **2018**, *130*, 6890–6895.
- [8] a) K. Y. Cheung, S. Gui, C. Deng, H. Liang, Z. Xia, Z. Liu, L. Chi, Q. Miao, *Chem* **2019**, *5*, 838–847; b) K. Y. Cheung, Y. Segawa, K. Itami, *Chem. Eur. J.* **2020**, *26*, 14791–14801.
- [9] a) P. J. Evans, N. Martín, *Chem* **2016**, *1*, 16–31; b) N. J. Schuster, R. H. Hernández Sánchez, D. Bukharina, N. A. Kotov, N. Berova, F. Ng, M. L. Steigerwald, C. A. Nuckolls, *J. Am. Chem. Soc.* **2018**, *140*, 6235–6239; c) S. Ma, J. Gu, C. Lin, Z. Luo, Y. Zhu, J. Wang, *J. Am. Chem. Soc.* **2020**, *142*, 16887–16893.
- [10] a) K. Kato, Y. Segawa, L. T. Scott, K. A. Itami, *Angew. Chem. Int. Ed.* **2018**, *57*, 1337–1341; *Angew. Chem.* **2018**, *130*, 1351–1355; b) F. Zhang, E. Michail, F. Saal, A.-M. Krause, P. Ravat, *Chem. Eur. J.* **2019**, *25*, 16241–16245; c) Y. Zhu, X. Guo, Y. Li, J. Wang, *J. Am. Chem. Soc.* **2019**, *141*, 5511–5517.
- [11] a) C. M. Cruz, I. R. Márquez, S. Castro-Fernández, J. M. Cuerva, E. Mações, A. G. Campaña, *Angew. Chem. Int. Ed.* **2019**, *58*, 8068–8072; *Angew. Chem.* **2019**, *131*, 8152–8156; b) M. M. Martín, F. Hampel, N. Jux, *Chem. Eur. J.* **2020**, *26*, 10210–10212; c) M. A. Medel, R. Tapia, V. Blanco, D. Miguel, S. P. Morcillo, A. G. Campaña, *Angew. Chem. Int. Ed.* **2021**, *60*, 6094–6100; *Angew. Chem.* **2021**, *133*, 6159–6165; d) P. Izquierdo-García, J. M. Fernández-García, I. Fernández, J. Perles, N. Martín, *J. Am. Chem. Soc.* **2021**, *143*, 11864–11870.
- [12] a) A. Narita, X. Wang, X. Feng, K. Müllen, *Chem. Soc. Rev.* **2015**, *44*, 6616–6643; b) X.-Y. Wang, X. Yao, A. Narita, K. Müllen, *Acc. Chem. Res.* **2019**, *52*, 2491–2505.
- [13] a) Y.-T. Wu, J. S. Siegel, *Chem. Rev.* **2006**, *106*, 4843–4867; b) M. Rickhaus, M. Mayor, M. Juríček, *Chem. Soc. Rev.* **2017**, *46*, 1643–1660; c) S. H. Pun, Q. Miao, *Acc. Chem. Res.* **2018**, *51*, 1630–1642; d) M. A. Majewski, M. Stepien, *Angew. Chem. Int. Ed.* **2019**, *58*, 86–116; *Angew. Chem.* **2019**, *131*, 90–122; e) J. Urieta-Mora, M. Krug, W. Alex, J. Perles, I. Fernández, A. Molina-Ontoria, D. M. Guldi, N. Martín, *J. Am. Chem. Soc.* **2020**, *142*, 4162–4172; f) S. Matsubara, Y. Koga, Y. Segawa, K. Murakami, K. Itami, *Nat. Catal.* **2020**, *3*, 710–718; g) S. Escayola, A. Poater, A. Muñoz-Castro, M. Solà, *Chem. Commun.* **2021**, *57*, 3087–3090.
- [14] a) K. Kawasumi, Q. Zhang, Y. Segawa, L. T. Scott, K. A. Itami, *Nat. Chem.* **2013**, *5*, 739–744; b) K. Kato, Y. Segawa, L. T. Scott, K. Itami, *Chem. Asian J.* **2015**, *10*, 1635–1639; c) J. Liu, S. Mishra, C. A. Pignedoli, D. Passerone, J. I. Urgel, A. Fabrizio, T. G. Lohr, J. Ma, H. Komber, M. Baumgarten, C. Corminboeuf, R. Berger, P. Ruffieux, K. Müllen, R. Fasel, X. Feng, *J. Am. Chem. Soc.* **2019**, *141*, 12011–12020; d) Y. Fei, Y. Fu, X. Bai, L. Du, Z. Li, H. Komber, K.-H. Low, S. Zhou, D. L. Phillips, X. Feng, J. Liu, *J. Am. Chem. Soc.* **2021**, *143*, 2353–2360.
- [15] J. M. Fernández-García, P. J. Evans, S. Medina Rivero, I. Fernández, D. García-Fresnadillo, J. Perles, J. Casado, N. Martín, *J. Am. Chem. Soc.* **2018**, *140*, 17188–17196.
- [16] a) A. Roth, C. Schierl, A. Ferrer-Ruiz, M. Minameyer, L. Rodríguez-Pérez, C. Villegas, M. A. Herranz, N. Martín, D. M. Guldi, *Chem* **2017**, *3*, 164–173; b) T. Scharl, A. Ferrer-Ruiz, A. Saura-Sanmartín, L. Rodríguez-Pérez, M. A. Herranz, N. Martín, D. M. Guldi, *Chem. Commun.* **2019**, *55*, 3223–3226; c) M. Garrido, M. K. Volland, P. W. Münich, L. Rodríguez-Pérez, J. Calbo, E. Ortí, M. A. Herranz, N. Martín, D. M. Guldi, *J. Am. Chem. Soc.* **2020**, *142*, 1895–1903; d) A. Stergiou, N. Tagmatarchis, *Small* **2021**, *17*, 2006005.
- [17] a) D. Canevet, E. M. Pérez, N. Martín, *Angew. Chem. Int. Ed.* **2011**, *50*, 9248–9259; *Angew. Chem.* **2011**, *123*, 9416–9427; b) M. Gallego, J. Calbo, J. Aragón, R. M. Krick Calderon, F. H. Liquido, T. Iwamoto, A. K. Greene, E. A. Jackson, E. M. Pérez, E. Ortí, D. M. Guldi, L. T. Scott, N. Martín, *Angew. Chem. Int. Ed.* **2014**, *53*, 2170–2175; *Angew. Chem.* **2014**, *126*, 2202–2207; c) H. Isla, E. M. Pérez, N. Martín, *Angew. Chem. Int. Ed.* **2014**, *53*, 5629–5633; *Angew. Chem.* **2014**, *126*, 5735–5739; d) E. M. Pérez, N. Martín, *Chem. Soc. Rev.* **2015**, *44*, 6425–6433.
- [18] a) A. D. Becke, *Phys. Rev. A* **1988**, *38*, 3098–3100; b) C. Lee, W. Yang, R. G. Parr, *Phys. Rev. B* **1988**, *37*, 785–789; c) F. Weigend, R. Ahlrichs, *Phys. Chem. Chem. Phys.* **2005**, *7*, 3297–3305.
- [19] a) A. J. Stasyuk, O. A. Stasyuk, M. Solà, A. A. Voityuk, *J. Phys. Chem. C* **2019**, *123*, 16525–16532; b) A. J. Stasyuk, O. A. Stasyuk, M. Solà, A. A. Voityuk, *J. Phys. Chem. B* **2020**, *124*, 9095–9102.
- [20] E. R. Johnson, S. Keinan, P. Mori-Sánchez, J. Contreras-García, A. J. Cohen, W. Yang, *J. Am. Chem. Soc.* **2010**, *132*, 6498–6506.
- [21] a) T. Yanai, D. P. Tew, N. C. Handy, *Chem. Phys. Lett.* **2004**, *393*, 51–57; b) P. Besalú-Sala, A. A. Voityuk, J. M. Luis, M. Solà, *Phys. Chem. Chem. Phys.* **2021**, *23*, 5376–5384.
- [22] a) J. Tomasi, B. Mennucci, R. Cammi, *Chem. Rev.* **2005**, *105*, 2999–3094; b) A. A. Voityuk, S. F. Vyboishchikov, *Phys. Chem. Chem. Phys.* **2019**, *21*, 18706–18713; c) A. A. Voityuk, S. F. Vyboishchikov, *Phys. Chem. Chem. Phys.* **2020**, *22*, 14591–14598.
- [23] R. A. Marcus, N. Sutin, *Biochim. Biophys. Acta Bioenerg.* **1985**, *811*, 265–322.

- [24] **NG-1** is the major fluorophore in the mixtures of **NG-1** and C_{60} . However, at the excitation wavelength 460 nm C_{60} possesses non-zero absorption, which eventually leads to inner filter effects.
- [25] D. M. Guldi, M. Prato, *Acc. Chem. Res.* **2000**, *33*, 695–703.
- [26] T. Kato, T. Kodama, T. Shida, T. Nakagawa, Y. Matsui, S. Suzuki, H. Shiromaru, K. Yamauchi, Y. Achiba, *Chem. Phys. Lett.* **1991**, *180*, 446–450.
- [27] Any attempts to fit the data under the assumption that it is the singlet excited state rather than the triplet excited state of **NG-1**, which interacts with C_{60} , failed as it provided unreasonable results.
- [28] a) G. J. Kavarnos, N. J. Turro, *Chem. Rev.* **1986**, *86*, 401–449;
b) C. Turró, J. M. Zaleski, Y. M. Karabatsos, D. G. Nocera, *J. Am. Chem. Soc.* **1996**, *118*, 6060–6067.

Manuscript received: September 21, 2021

Accepted manuscript online: October 11, 2021

Version of record online: December 29, 2021